Loading condition estimation using long-period fiber grating array

Felipe Oliveira Barino, Renato Faraco-Filho, Deivid Campos, Vinicius N. H. Silva, Andrés P. López-Barbero, Leonardo Honório, and Alexandre Bessa dos Santos

***Abstract*—To ensure the safety and durability of structures, the constant monitoring of their structural health has been used by engineers to manage these structures. Optical fiber sensors have the advantage of long transducer-to-processing distances, the capacity to work in harsh environments, immunity to electromagnetic noise, and reliability. Therefore, optical fiber sensors are great candidates to monitor structures in-service. Here, we propose the use of a long-period fiber grating (LPG) array to monitor the loading condition of a structure. The identification method was tested in a simply-supported beam model and the estimated loading conditions were compared to the loading conditions applied to the beam. By analyzing different combinations of force intensity and position along the beam length, the results showed the force position could be estimated with 0.901% accuracy and force intensity with 2.51% accuracy using a four-LPG strain sensor array.**

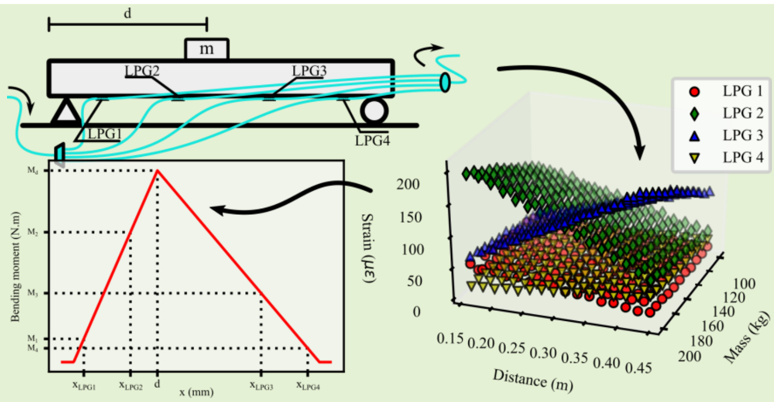

***Index Terms*—strain sensor, structural health monitoring, force sensing, optical sensor, arc-induced**

I. Introduction

STRUCTURES such as bridges, electro-towers, railroads, pavements, and buildings suffer from continuous loading and environmental action, leading to degradation and structural damage. To increase the safety and durability of such structures, engineers have been employing structural health monitoring (SHM) systems to continuously monitor structures. In such systems, we can highlight the importance of displacement and deformation sensors. Most of the literature on SHM is based on resistive strain gauges [1]–[5], but this type of strain sensor presents some disadvantages such as low signal-to-noise ratio (SNR), high signal attenuation, high-temperature cross-sensitivity, and need for multiple wires for power and signal.

To overcome these drawbacks, some authors proposed the use of piezoelectric materials to manufacture sensors for SHM, due to its high sensitivity, self-powering ability, and fast response [6]–[9]. And although the use of piezoelectric devices could improve the SNR and reduce the wiring [10], these devices still are based on electric signals that are susceptible to electromagnetic interference and high attenuation for long-distance applications.

The remarkable work of Butter and Hocker in 1978 [11] introduced the first optical alternative to electric strain gauges. While electrical strain gauges are highly susceptible to electromagnetic noise and need a wide number of cables, fiber-optic strain gauges are immune to electromagnetic noise and can be easily multiplexed in a single fiber optic cable that can transmit the sensing signal for several kilometers with little attenuation and without degradation from electromagnetic interference.

Since then, the use of optical sensors in SHM systems has been reported in the literature for various applications. Optical fiber sensors have been used in crack monitoring [12], [13]; and fiber Bragg gratings have been played an important role in the structural health monitoring of bridges [14]–[17] and

This work was supported in part by the Programa de Bolsas de Pós-graduação (PBPG-UFJF) through the Programa de Pós-graduação em Engenharia Elétrica (PPEE-UFJF), Coordenação de Aperfeiçoamento Pessoal de Nível Superior (CAPES), Conselho Nacional de Desenvolvimento Científico e Tecnológico (CNPq), Instituto Nacional de Energia Elétrica (Inerge-UFJF), BAESA, ENERCAN, and FOZ DO CHAPECÓ, under the supervision of Agência Nacional de Energia Elétrica (ANEEL).

Felipe Oliveira Barino is with the Department of Circuits, Federal University of Juiz de Fora (UFJF), 36036-900, Brazil (e-mail: felipe.barino@engenharia.ufjf.br).

Renato Luiz Faraco-Filho is with the Department of Circuits, Federal University of Juiz de Fora (UFJF), 36036-900, Brazil.

Deivid Campos is with the Department of Mechanics, Federal University of Juiz de Fora (UFJF), 36036-900, Brazil.

Vinicius N. H. Silva is with the Department of Telecommunications, Fluminense Federal University (UFF), 24220-900, Brazil.

Andrés P. López Barbero is with the Department of Telecommunications, Fluminense Federal University (UFF), 24220-900, Brazil.

Leonardo Honório is with the Department of Energy, Federal University of Juiz de For a (UFJF), 36036-900, Brazil

Alexandre Bessa dos Santos is with the Department of Circuits, Federal University of Juiz de For a (UFJF), 36036-900, Brazil

concrete structures [18]–[22].

A fiber Bragg grating is an in-fiber grating device manufactured by periodically changing the fiber's refractive index with a period in the order of hundreds of nanometers. This periodic structure couples the propagating core mode to a counter-propagating core mode and causes light to reflect at a specific wavelength [23]. Due to the submicrometric structure of the FBGs, its fabrication is difficult and often requires expensive equipment. Long-period fiber gratings (LPGs) on the other hand, are in-fiber grating devices manufactured by periodic changes in the fiber's refractive index and/or geometry in the order of hundreds to thousands of micrometers and, therefore, LPGs can be easily manufactured by low-cost point-by-point techniques, using a fiber optic splicing machine for example [24].

LPGs have been widely used in telecommunications [25], [26] and sensing of various quantities [27]–[31]. Opposed to the FBGs, they are strictly transmission devices, the longer period causes light from the fundamental core mode to couple to a co-propagating cladding mode. The energy coupled to a cladding mode is lost by scattering at the cladding/external medium interface [23], forming rejection bands. Therefore, the LPG transmission characteristic is a notch filter centered at the wavelengths in which coupling occurred:

$$\lambda_{res}^{m} = \left(n_{eff,co} - n_{eff,cl}^{m}\right) \cdot \Lambda \quad (1)$$

where λ_{res}^{m} is the mth resonant wavelength, $n_{eff,co}$ and $n_{eff,cl}^{m}$ are the effective refractive index of the core and mth cladding mode, respectively, and Λ is the grating period.

LPGs are sensitive to deformation by two factors: (I) period change caused by deformation and (II) refractive index change caused by the photo-elastic effect. Let η_{co} and η_{cl} be the elasto-optic coefficient of the core and cladding material, respectively. Therefore, the resonant wavelength shift due to strain is given by [32]:

$$\frac{\mathrm{d}\lambda_{res}^{m}}{\mathrm{d}\epsilon} = \lambda_{res}^{m} \cdot \Lambda \cdot \left(1 + \frac{\eta_{co} n_{eff,co} - \eta_{cl} n_{eff,cl}^{m}}{n_{eff,co} - n_{eff,cl}^{m}}\right) \quad (2)$$

Hence, by tracking the LPG resonant wavelength one can establish the relative displacement or deformation at the device and use it as a strain transducer. And by placing this transducer at a given structure, continuous periodic measurements of strain can be made. This continuous strain measurement is the core of structural health monitoring (SHM) and is useful in several industries, such as aerospace, civil, and mechanical engineering [33]. Besides the low-cost fabrication, LPGs present higher static stress sensitivity and can be temperature insensitive, with a proper choice of operating cladding mode [32].

In this work, we investigate the use of LPG sensors in multi-point strain sensing as a low-cost alternative to FBG sensors, although the use of LPGs in SHM is mainly related to its refractive index sensitivity [34], [35], its high strain sensitivity could also be explored to measure strain. Although LPGs also present high sensitivity to other parameters that could introduce random fluctuations and wrong measurements due to cross-sensitivity, several works addressed and corrected this problem [36]–[38]. Moreover, comparing LPGs to FBGs, due to the LPG's complex spectrum and several resonant wavelengths, the spectral analysis of an LPG could be used to retrieve more information about the environment, leading to single-sensor multi-parameter sensing [39], that could also be used for cross-sensitivity compensation. Therefore, offering more processing possibilities than an FBG sensor.

We used four LPG sensors to monitor the strain in a simply supported beam and estimated the beam bending moment to determine the loading scenario, i.e. the force intensity and its position along the beam. This investigation could be a starting point for several concentrated load identification problems in beam structures; the study could be extended to dynamic and moving loads, offering a great solution to structural health monitoring of bridges and even traffic monitoring. To the best of our knowledge, the use of arrayed LPGs for loading condition estimation has never been addressed in the literature before and, therefore, this paper could favor the field of remote structures monitoring by presenting a low-cost optical fiber transducer alternative for civil engineers to monitor and collect data on these structures.

II. METHODS

We manufactured four LPG strain sensors in standard telecommunications single-mode fiber (SMF-28) by inducing a periodic modulation on the fiber index and radius using the arc-electric technique [24]. All four LPG sensors were manufactured with the same period Λ=430 μm and length L=12.9 mm using a splicing machine pre-tuned to ensure low average temperature and high temperature gradient, thus increasing the fabrication reproducibility [24]. Therefore, the

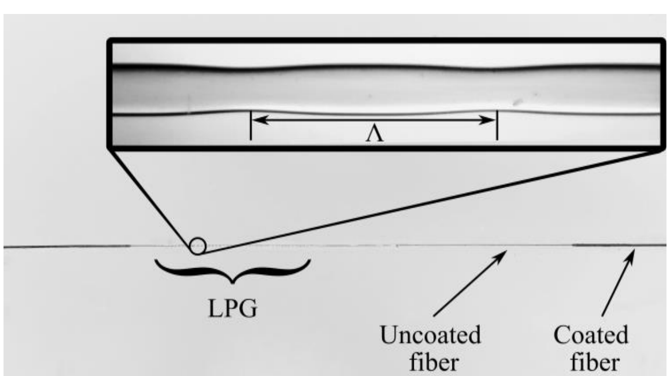

Fig. 1. One of the arc-induced LPG manufactured for strain measurements.

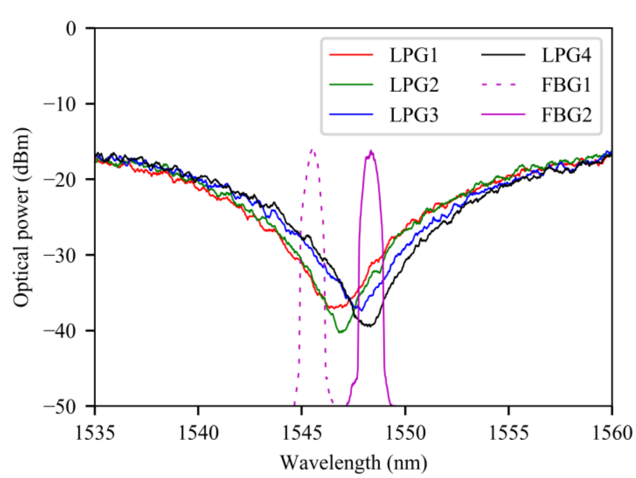

Fig. 2. Spectra of the sensing LPGs and FBGs of the interrogator.

wavelength response of all four sensors is similar. Fig. 1 shows photography of one of these LPG sensors and a micrography detailing the periodic structure, while Fig. 2 shows their transmission spectra.

The LPGs were illuminated by a broadband light source (BBS) and we used a 1x4 optical switch to select each LPG sensor individually. This optical setup can be seen in Fig. 3, where the experimental setup is schematized.

As shown in Fig. 3, the optical sensors were interrogated by two FBGs, kept in a temperature-controlled environment, using the FBG filtered power ratio to measure the strain [40]:

$$R = \frac{P_{FBG2} - P_{FBG1}}{P_{FBG2} + P_{FBG1}} \tag{3}$$

where R is the FBGs power ratio, P_{FBG1} is the power reflected by the FBG1 and P_{FBG2} is the power reflected by the FBG2. The reflection spectra of these FBGs can be seen in Fig. 2, their Bragg wavelengths are 1545.6 nm and 1548.4 nm for FBG1 and FBG2, respectively.

We calibrated the four LPG sensors for strain from 0 με to 150 με in 15 equally spaced values measured by a micrometer. We observed both the spectral shift and the FBG power ratio variation to determine the LPGs sensitivity to strain, using the former, and the interrogator output, using the latter.

Then, the four sensors were glued at the bottom of a 6351-T6 aluminum beam using epoxy glue. We made sure that the LPGs' periodic structure was centered at the desired sensing points and that the gluing points were not directly in contact to the LPGs themselves, only in unmodified bare fiber.

However, is important to emphasize that the LPGs are fragile and highly sensitive to the external refractive index. Although in this work the possibility of LPG failure or refractive index cross-sensitivity was minimized by the lab controlled environment, in a real-world application is important to cover and protect the LPGs. A simple, effective, customizable, and novel approach to this problem is the 3d printed encapsulation [41], [42]. This technique allows for easy adaptation to the sensing structure, low-cost fabrication, fast prototyping, and also facilitates the LPG installation.

The aluminum beam had 605 mm x 64 mm x 20 mm dimensions and was supported at 25 mm from both ends. The x coordinate for LPG1, LPG2, LPG3, and LPG4 was 50 mm, 155 mm, 450 mm, and 555 mm, respectively, measured from the beam edge.

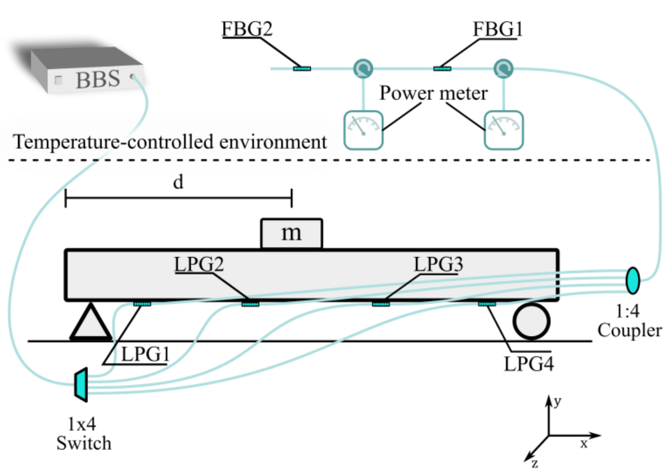

Fig. 3. Experimental setup scheme.

To emulate different a loading condition, we added a mass m at a distance d from the beam edge, as shown in Fig. 3. This procedure was repeated for several m x d combinations, the mass was varied from 100 kg to 200 kg and d from 160 mm to 445 mm.

The strain at each LPG sensor located at the (x, y, z) coordinate can be calculated by:

$$\epsilon(x, y) = \frac{M(x,y)y}{E\,I} \tag{4}$$

where $M(x, y)$ is the bending moment at the sensor location, E is the beam Young modulus, and I its moment of inertia. Consequently, we could retrieve the bending moment at the sensor location by the strain measurements. Moreover, the bending moment could be retrieved for all x if the applied force is between at least two points where the strain is known, given the piecewise linear characteristics of the simply supported beam bending moment.

For the loading scenario illustrated in Fig. 3, the bending moment is shown in Fig. 4. The bending moment for each sensor position is highlighted, as well as the bending moment at the mass position. Note that for all $x_{LPG2} < d < x_{LPG3}$ the bending moment could be estimated by tracing the line crossing the points (x_{LPG1}, M_1) and (x_{LPG2}, M_2) and the line crossing (x_{LPG3}, M_3) and (x_{LPG4}, M_4). Furthermore, once the bending moment is known, the mass position d can be easily determined, and the applied force (m times gravity acceleration) can be calculated by the bending moment M_d.

We measured the strain at the four LPGs and estimated the bending moment to recover the applied force and its position for each tested loading configuration. From the recovered values we estimate the proposed system performance by the root mean squared error (RMSE) and mean absolute error (MAE) of both position and force. We also simulated each loading condition using a finite element method (FEM) software to calculate the strain at each LPG and compare it to the measured by each sensor.

III. Results

The LPGs' calibration results can be seen in Fig. 5 and Fig. 6. The first shows the LPGs response to strain in terms of their resonant wavelength, whereas the second shows the relationship between the applied strain and the FBGs power

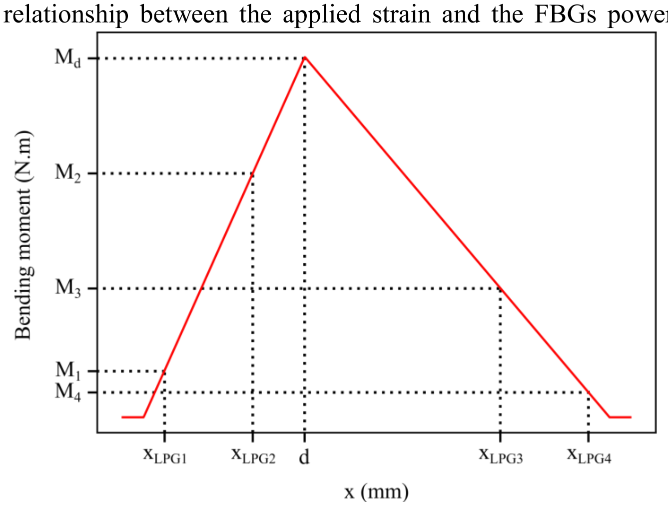

Fig. 4. Example of bending moment diagram, with sensor and force location highlighted.

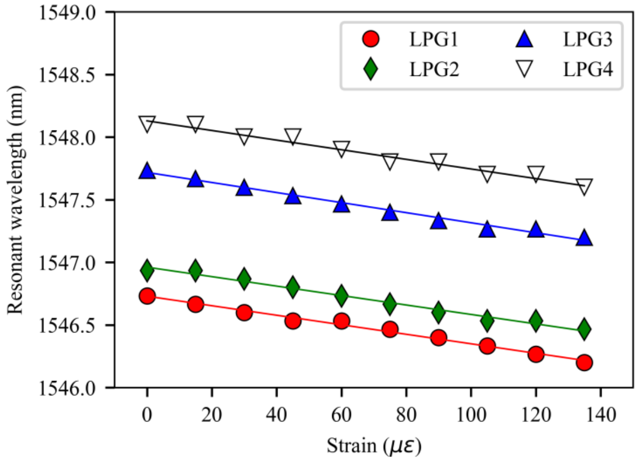

Fig. 5. Relationship between strain and the LPG resonant wavelength.

TABLE I
LPGS SENSITIVITY TO STRAIN.

	Sensitivity (pm/με)	R^2
LPG1	-3.798	0. 9893
LPG2	-3.771	0. 9833
LPG3	-4.013	0. 9879
LPG4	-3.838	0. 9733

ratio, i.e. the interrogated response of the LPGs to strain.

From the fitted curves seen in Fig. 5, we obtained the sensitivities and R^2 shown in Table I, and the results showed the LPG sensors had high sensitivity to strain and high linearity, given the R^2 close to one.

The calibration results with respect to the FBG power ratio can be seen in Fig. 6. In this case, the calibration curves of all sensors also exhibited a highly linear behavior with R^2 of 0.9989, 0.9979, 0.9996, and 0.9931, for LPG 1, LPG 2, LPG 3, and LPG 4, respectively.

Using the interrogator calibration curves showed in Fig. 6, we measured the strain for all loading conditions tested. The results are summarized in Fig. 7. Note that each strain measurement combination is related to a loading condition, i.e.

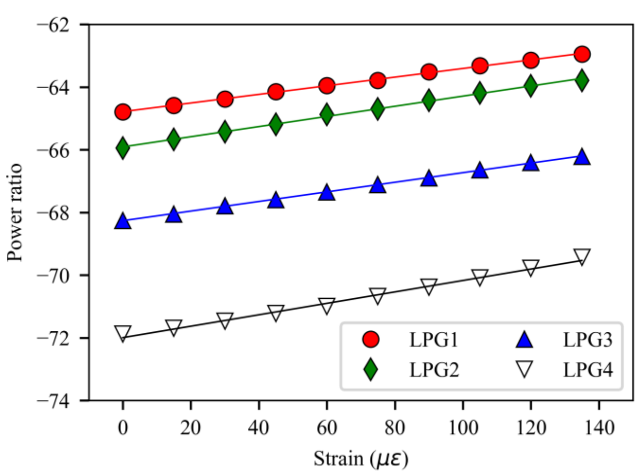

Fig. 6. Relationship between strain and the FBGs power ratio.

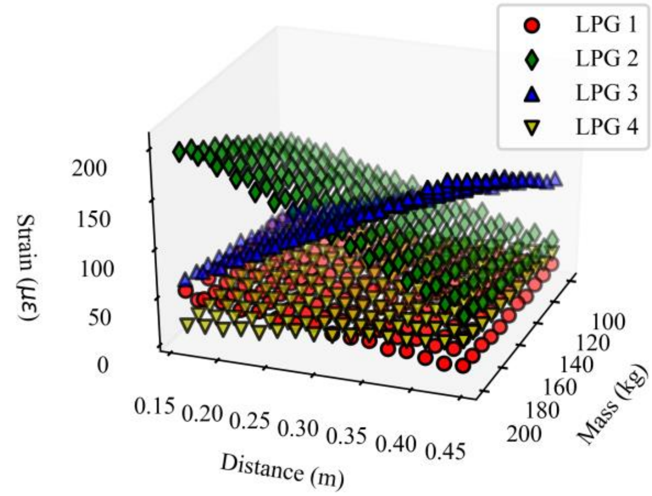

Fig. 7. Relationship between mass (m), distance (d) and strain at each LPG sensor.

a single pair of m and d.

We could see that the strain measured by the LPGs increased with the mass in all sensing points. We also noted that for LPG 1 and LPG 2, the strain is inversely proportional to the distance, while it is proportional to the distance for LPG 3 and LPG 4.

These tested loading conditions were simulated and the measured strain was compared to the simulated strain, this comparison can be seen in Fig. 8, where the x-axis represents the experimental strain and the y-axis the FEM simulation results. Note that this plot is close to the identity linear function, therefore indicating the measured strain agrees to the simulated strain.

Tracing the bending moment for each distance and mass combination shown in Fig. 7 we were able to determine the force position with 7.6 mm RMSE and 5.5 mm MAE, this represents 1.26% and 0.901% of the beam length, respectively. Whereas the force intensity was estimated with 64 N RMSE and 49 N MAE, representing 3.28% and 2.51% of the maximum applied force. A comparison between the estimated position and force is summarized in Fig. 9, where the black axis and points represents the force position,

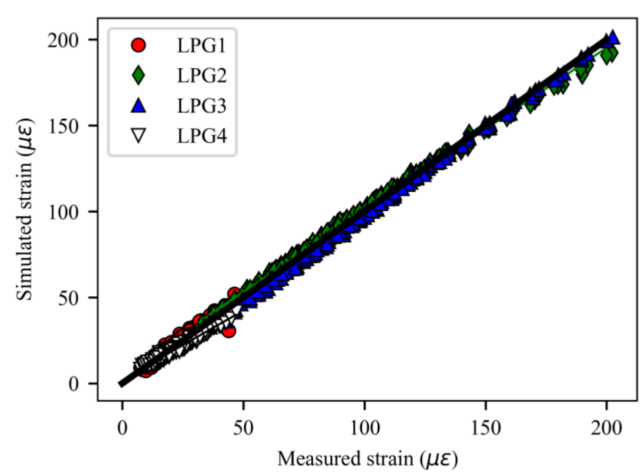

Fig. 8. Comparison between the strain measured and the FEM simulation.

whereas the red axis and points represents the force intensity. The line showed in this figure is the $y = x$ function, therefore indicating the perfect estimation.

From Fig. 9 we could see a small drift on the estimated position towards lower values when $d < 200$ mm, where the points are at the straight line left-hand side. On the other hand, analysis of the force intensity showed a sub-estimation of force intensity in all tested cases, with several points at the straight line left-hand side. Indeed, we could see bigger errors in force intensity identification, with more than two times the position identification percentage error.

From Fig. 8 we observed that the points drifted towards smaller values when the measured strain was small. Therefore, when the measured strain is small, the sensors tended to overestimate the strain, in comparison to the simulated strain. Since smaller strain leads to smaller bending moment and the LPGs closer to the beam edges, i.e. LPG1 and LPG4, are susceptible to smaller strain than the central ones, the overestimation of the bending moment at these points could lead to the sub-estimation of the applied force when tracing the bending moment curve.

To illustrate these results of loading condition estimation, four randomly selected samples can be seen in Fig. 10, where

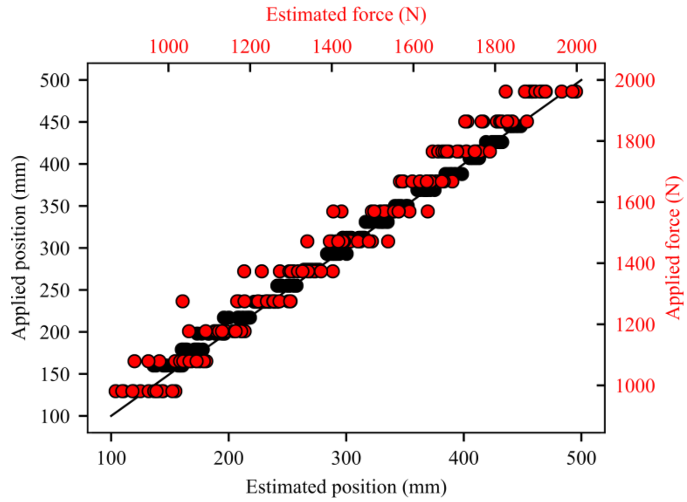

Fig. 9. Comparison between estimated and real values for force (red) and position (black).

the bending moment applied to the beam is compared to the estimated using the LPG sensor array. Table II shows the estimated force position and intensity in comparison to the applied values for each of the four examples showed in

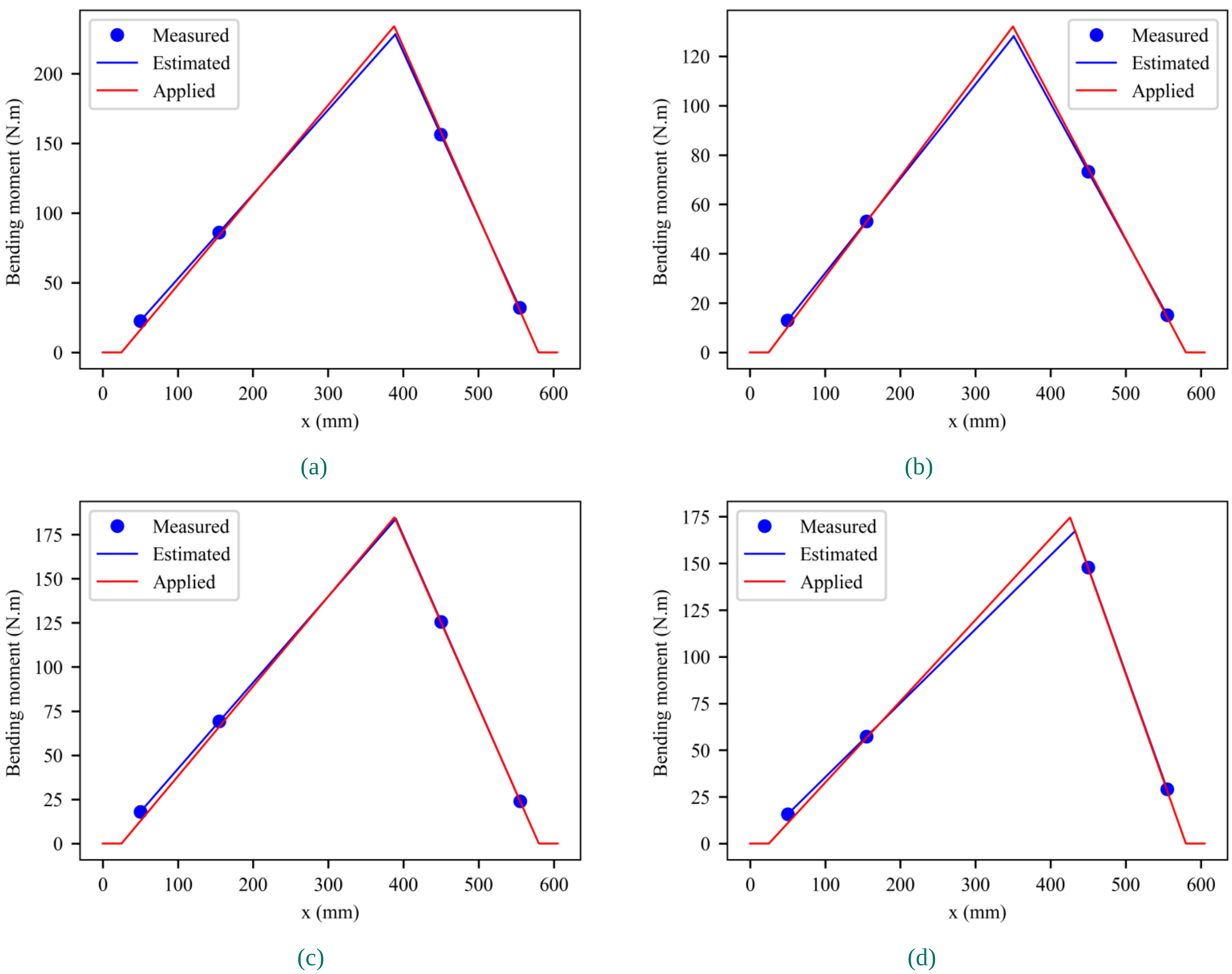

Fig. 10. Bending moment estimation based on strain measured by the four LPGs. Loading conditions are summarized in Table II.

TABLE II
COMPARISON BETWEEN REAL AND ESTIMATED LOADING CONDITIONS SHOWED IN FIG. 10.

	Position (mm)		Intensity (N)	
	Real	Estimated	Real	Estimated
(a)	388.0	389.5	1863.9	1816.4
(b)	350.0	351.0	981.0	951.5
(c)	388.0	389.8	1471.5	1464.1
(d)	426.0	432.6	1569.6	1504.1

Fig. 10. Note that the bending moment measured by the LPG1 was over-estimated in all cases illustrated in this figure, leading to the bending moment peak sub-estimation, which was used to calculate the applied force.

IV. CONCLUSION

In this paper, we demonstrated the use of LPGs in multi-point strain measurement and the application of the measured strain to identify static loading conditions. We tested the loading condition identification system for several different scenarios and evaluated the RMSE and MAE for both force position and intensity.

Although the four strain sensors approach to load condition estimation is the minimal required for estimating the bending moment, the results showed low RMSE and MAE, especially for force position. It is important to note that minor fluctuations on the measured strain could impact in a large deviation of the lines connecting each measured bending moment points, resulting in poor bending moment estimation. Therefore, incorporating more points, by using more LPG sensors and a least square method to fit the bending moment piecewise function could improve the load condition estimation.

REFERENCES

[1] J. dos Reis, C. Oliveira Costa, and J. Sá da Costa, "Double bridge circuit for self-validated structural health monitoring strain measurements," *Strain*, vol. 54, no. 5, p. e12278, Oct. 2018, doi: 10.1111/str.12278.

[2] Y. Zhang, N. Anderson, S. Bland, S. Nutt, G. Jursich, and S. Joshi, "All-printed strain sensors: Building blocks of the aircraft structural health monitoring system," *Sensors Actuators A Phys.*, vol. 253, pp. 165–172, 2017, doi: https://doi.org/10.1016/j.sna.2016.10.007.

[3] M. Vafaei and S. C. Alih, "An Ideal strain gage placement plan for structural health monitoring under seismic loadings," *Earthquakes Struct.*, vol. 8, no. 3, pp. 541–553, Mar. 2015, doi: 10.12989/eas.2015.8.3.541.

[4] A. K. Bose *et al.*, "Highly Sensitive Screen Printed Strain Gauge for Micro-Strain Detection," in *2019 IEEE International Conference on Flexible and Printable Sensors and Systems (FLEPS)*, Jul. 2019, pp. 1–3, doi: 10.1109/FLEPS.2019.8792282.

[5] Haksoo Choi, Sukwon Choi, and Hojung Cha, "Structural Health Monitoring system based on strain gauge enabled wireless sensor nodes," in *2008 5th International Conference on Networked Sensing Systems*, Jun. 2008, pp. 211–214, doi: 10.1109/INSS.2008.4610888.

[6] A. S. Babaev and I. V. Yanchevskii, "Identification of external load and control of deformed state of an asymmetric trimorphic beam in unsteady modes," *Mech. Solids*, vol. 48, no. 6, pp. 697–705, Nov. 2013, doi: 10.3103/S0025654413060125.

[7] H. Zhang, M. Shen, Y. Zhang, Y. Chen, and C. Lü, "Identification of Static Loading Conditions Using Piezoelectric Sensor Arrays," *J. Appl. Mech.*, vol. 85, no. 1, Jan. 2018, doi: 10.1115/1.4038426.

[8] Y. Chen *et al.*, "Mechanical Energy Harvesting From Road Pavements Under Vehicular Load Using Embedded Piezoelectric Elements," *J. Appl. Mech.*, vol. 83, no. 8, Aug. 2016, doi: 10.1115/1.4033433.

[9] J. H. Wang and C. Q. Chen, "Effects of Thickness on the Responses of Piezoresponse Force Microscopy for Piezoelectric Film/Substrate Systems," *J. Appl. Mech.*, vol. 84, no. 12, Dec. 2017, doi: 10.1115/1.4038064.

[10] J. Sirohi and I. Chopra, "Fundamental Understanding of Piezoelectric Strain Sensors," *J. Intell. Mater. Syst. Struct.*, vol. 11, no. 4, pp. 246–257, Apr. 2000, doi: 10.1106/8BFB-GC8P-XQ47-YCQ0.

[11] C. D. Butter and G. B. Hocker, "Fiber optics strain gauge," *Appl. Opt.*, vol. 17, no. 18, p. 2867, Sep. 1978, doi: 10.1364/AO.17.002867.

[12] K. S. C. Kuang, Akmaluddin, W. J. Cantwell, and C. Thomas, "Crack detection and vertical deflection monitoring in concrete beams using plastic optical fibre sensors," *Meas. Sci. Technol.*, vol. 14, no. 2, pp. 205–216, Feb. 2003, doi: 10.1088/0957-0233/14/2/308.

[13] J. Zhao, T. Bao, and U. Amjad, "Optical fiber sensing of small cracks in isotropic homogeneous materials," *Sensors Actuators A Phys.*, vol. 225, pp. 133–138, Apr. 2015, doi: 10.1016/j.sna.2015.02.017.

[14] T. H. T. Chan *et al.*, "Fiber Bragg grating sensors for structural health monitoring of Tsing Ma bridge: Background and experimental observation," *Eng. Struct.*, vol. 28, no. 5, pp. 648–659, Apr. 2006, doi: 10.1016/j.engstruct.2005.09.018.

[15] R. C. Tennyson, A. A. Mufti, S. Rizkalla, G. Tadros, and B. Benmokrane, "Structural health monitoring of innovative bridges in Canada with fiber optic sensors," *Smart Mater. Struct.*, vol. 10, no. 3, pp. 560–573, Jun. 2001, doi: 10.1088/0964-1726/10/3/320.

[16] Y. Bin Lin, C. L. Pan, Y. H. Kuo, K. C. Chang, and J. C. Chern, "Online monitoring of highway bridge construction using fiber Bragg grating sensors," *Smart Mater. Struct.*, vol. 14, no. 5, pp. 1075–1082, Oct. 2005, doi: 10.1088/0964-1726/14/5/046.

[17] D. Li, Z. Zhou, and J. Ou, "Development and sensing properties study of FRP–FBG smart stay cable for bridge health monitoring applications," *Measurement*, vol. 44, no. 4, pp. 722–729, May 2011, doi: 10.1016/j.measurement.2011.01.005.

[18] Y. Bin Lin, K. C. Chang, J. C. Chern, and L. A. Wang, "The health monitoring of a prestressed concrete beam by using fiber Bragg grating sensors," *Smart Mater. Struct.*, vol. 13, no. 4, pp. 712–718, Aug. 2004, doi: 10.1088/0964-1726/13/4/008.

[19] P. Moyo, J. M. W. Brownjohn, R. Suresh, and S. C. Tjin, "Development of fiber Bragg grating sensors for monitoring civil infrastructure," *Eng. Struct.*, vol. 27, no. 12, pp. 1828–1834, Oct. 2005, doi: 10.1016/j.engstruct.2005.04.023.

[20] M. A. Davis, D. G. Bellemore, and A. D. Kersey, "Distributed fiber Bragg grating strain sensing in reinforced concrete structural components," *Cem. Concr. Compos.*, vol. 19, no. 1, pp. 45–57, Jan. 1997, doi: 10.1016/S0958-9465(96)00042-X.

[21] M. H. Maher and E. G. Nawy, "Evaluation of fiber optic Bragg grating strain sensor in high strength concrete beams," in *Applications of Fiber Optic Sensors in Engineering Mechanics*, 1993, pp. 120–133.

[22] L.-H. Kang, D.-K. Kim, and J.-H. Han, "Estimation of dynamic structural displacements using fiber Bragg grating strain sensors," *J. Sound Vib.*, vol. 305, no. 3, pp. 534–542, Aug. 2007, doi: 10.1016/j.jsv.2007.04.037.

[23] H. A. Haus and W. Huang, "Coupled-mode theory," *Proc. IEEE*, vol. 79, no. 10, pp. 1505–1518, 1991, doi: 10.1109/5.104225.

[24] G. Rego, "Arc-Induced Long Period Fiber Gratings," *J. Sensors*, vol. 2016, pp. 1–14, 2016, doi: 10.1155/2016/3598634.

[25] J. Wei, M.-Y. Chen, Q. Xiang, and R. Huang, "Design of a mode-field converter based on a two-core optical fiber with a long-period fiber grating," *Opt. Eng.*, vol. 55, no. 6, p. 066110, Jun. 2016, doi: 10.1117/1.OE.55.6.066110.

[26] B. Huang, H. Chen, N. K. Fontaine, R. Ryf, I. Giles, and G. Li, "Large-bandwidth, low-loss, efficient mode mixing using long-period mechanical gratings," *Opt. Lett.*, vol. 42, no. 18, p. 3594, Sep. 2017, doi: 10.1364/OL.42.003594.

[27] Y. Chen, F. Tang, Y. Bao, Y. Tang, and G. Chen, "A Fe-C coated long-period fiber grating sensor for corrosion-induced mass loss measurement," *Opt. Lett.*, vol. 41, no. 10, p. 2306, May 2016, doi: 10.1364/OL.41.002306.

[28] F. Delgado and A. Bessa, "Torsion-dependent spectral response of long-period fiber grating based on electric arc technique with axial rotation of the fiber," *Microw. Opt. Technol. Lett.*, vol. 61, no. 1, pp. 178–181, Jan. 2019, doi: 10.1002/mop.31532.

[29] C. Du, Y. Zhao, Q. Wang, and F. Xia, "Sensitivity-optimized long-period fiber gratings for refractive index and temperature sensing," *Instrum. Sci. Technol.*, vol. 46, no. 4, pp. 435–449, Jul. 2018, doi: 10.1080/10739149.2017.1395744.

[30] F. Barino, F. S. Delgado, M. A. Jucá, T. V. N. Coelho, and A. Bessa dos Santos, "Comparison of regression methods for transverse load sensor based on optical fiber long-period grating," *Measurement*, vol. 146, pp. 728–735, Nov. 2019, doi: 10.1016/j.measurement.2019.07.017.

[31] Y.-L. Yu, H.-H. Hung, S.-K. Liaw, M.-H. Shih, H. Kishikawa, and N. Goto, "Simultaneously two-parameter measurement using tilted fiber grating and long period fiber grating," *Microw. Opt. Technol. Lett.*, vol. 59, no. 5, pp. 1122–1125, May 2017, doi: 10.1002/mop.30479.

[32] Xuewen Shu, Lin Zhang, and I. Bennion, "Sensitivity characteristics of long-period fiber gratings," *J. Light. Technol.*, vol. 20, no. 2, pp. 255–266, 2002, doi: 10.1109/50.983240.

[33] C. R. Farrar and K. Worden, "An introduction to structural health monitoring," *Philos. Trans. R. Soc. A Math. Phys. Eng. Sci.*, vol. 365, no. 1851, pp. 303–315, Feb. 2007, doi: 10.1098/rsta.2006.1928.

[34] S. Zheng, "Long-period fiber grating moisture sensor with nano-structured coatings for structural health monitoring," *Struct. Heal. Monit. An Int. J.*, vol. 14, no. 2, pp. 148–157, Mar. 2015, doi: 10.1177/1475921714560069.

[35] Y. Huang, F. Tang, X. Liang, G. Chen, H. Xiao, and F. Azarmi, "Steel bar corrosion monitoring with long-period fiber grating sensors coated with nano iron/silica particles and polyurethane," *Struct. Heal. Monit. An Int. J.*, vol. 14, no. 2, pp. 178–189, Mar. 2015, doi: 10.1177/1475921714560070.

[36] M. N. Ng, Z. Chen, and K. S. Chiang, "Temperature compensation of long-period fiber grating for refractive-index sensing with bending effect," *IEEE Photonics Technol. Lett.*, 2002, doi: 10.1109/68.986813.

[37] Y.-P. Wang, L. Xiao, D. N. Wang, and W. Jin, "Highly sensitive long-period fiber-grating strain sensor with low temperature sensitivity," *Opt. Lett.*, 2006, doi: 10.1364/ol.31.003414.

[38] C. Trono, F. Baldini, M. Brenci, F. Chiavaioli, and M. Mugnaini, "Flow cell for strain- and temperature-compensated refractive index measurements by means of cascaded optical fibre long period and Bragg gratings," *Meas. Sci. Technol.*, 2011, doi: 10.1088/0957-0233/22/7/075204.

[39] F. S. Delgado and A. B. dos Santos, "Multi-measurement scheme for a fiber-optic sensor based on a single long-period grating," *J. Mod. Opt.*, vol. 64, no. 21, pp. 2428–2432, Nov. 2017, doi: 10.1080/09500340.2017.1367854.

[40] H. J. Patrick, G. M. Williams, A. D. Kersey, J. R. Pedrazzani, and A. M. Vengsarkar, "Hybrid fiber Bragg grating/long period fiber grating sensor for strain/temperature discrimination," *IEEE Photonics Technol. Lett.*, vol. 8, no. 9, pp. 1223–1225, Sep. 1996, doi: 10.1109/68.531843.

[41] P. Di Palma, A. Iadicicco, and S. Campopiano, "Study of fiber Bragg gratings embedded in 3D-printed patches for deformation monitoring," *IEEE Sens. J.*, pp. 1–1, 2020, doi: 10.1109/JSEN.2020.3004280.

[42] W. Yan, S. Ma, H. Wang, and X. Zhang, "Fiber Bragg grating online packaging technology based on 3D printing," *Opt. Laser Technol.*, vol. 131, p. 106443, Nov. 2020, doi: 10.1016/j.optlastec.2020.106443.

Felipe O. Barino was born in Juiz de Fora, Brazil, in 1996. He received his B.Sc. degree in electronics from the Federal University of Juiz de Fora (UFJF), Minas Gerais, Brazil, in 2019 and is now pursuing his M.Sc. degree in electrical engineering at Programa de Pós Graduação em Engenharia Elétrica - PPEE/UFJF. His current research interests are related to instrumentation, optical fiber sensors, and machine learning.

Renato Faraco-Filho was born in Conselheiro Lafaiete Brazil, in 1997. He is an undergraduate student in electrical engineering and electronics systems in Federal University of Juiz de Fora, pursuing his B. Sc. degree. His current research interests are related to instrumentation, optical fiber sensor, and computational methods.

Deivid Campos was born in São João Nepomuceno, Brazil, in 1991. He received his B.Sc degree in Exact Sciences from the Federal University of Juiz de Fora (UFJF), Minas Gerais, Brazil, in 2014 and now seeks his B.Sc. in Mechanical Engineering at UFJF. His current research interests are related to instrumentation, fiber optic sensors, and three-dimensional modeling with 3D printing.

Vinicius N. H. Silva was born in Niterói, Brazil, in 1979. He received the M.Sc. degree in telecommunication engineering from Federal Fluminense University (UFF), Niterói, in 2009, and the Ph.D. degree in telecommunication engineering from Télécom Bretagne, France, in 2013. Since 2014, he has been an Associate Professor with the Telecommunication Engineering Department, Federal Fluminense University (UFF). His research interests include turbulence effects in free-space optics, optical fiber sensors, and optical communications.

Andrés P. López-Barbero was born in Montevideo, Uruguay, in 1966. He received the M.Sc. degree in optical engineering from the Technological Institute of Aeronautics (ITA), São Paulo, Brazil, in 1994, and the Ph.D. degree in electrical engineering from Campinas State University (UNICAMP), São Paulo, in 2000. Since 1989, he has been an Associate Professor with the Telecommunication Engineering Department, Federal Fluminense University (UFF), Niterói, Brazil. His research interests include optical fiber sensors, optical communications, and sensors for electric power networks.

Leonardo de Mello Honório was born in Juiz de Fora, Brazil, in 1971. He received the B.Sc. degree from the Federal University of Juiz de Fora (UFJF), in 1993, and the M.Sc. and Ph.D. degrees from EFEI, Brazil, in 1999 and 2002, respectively, all in electrical engineering. He was a Visiting Researcher with Porto and Irvine California University, in 2006 and 2012, respectively. He is currently an Associate Professor with UFJF. His current research interests include evolutionary algorithms, probabilistic methods, optimal power flow, robotics, autonomous vehicles, fuzzy logic, pattern recognition, and optimization.

Alexandre Bessa dos Santos was born in Juiz de Fora, Brazil, in 1975. He received the M.Sc. and Ph.D. degrees in electrical engineering from Pontifical Catholic University (PUC), Brazil, in 2001 and 2005, respectively. Since 2010, he has been an Associated Professor with the Department of Circuits at Federal University of Juiz de Fora (UFJF), Juiz de Fora. His research interests include applied electromagnetism, optical sensors, computational methods, instrumentation, and metrology.